proceedings

Abstract

Laser thermography as non-destructive technique to detect defects in AlSi10Mg parts printed with L-PBF process †

Ester D'Accardi [1], Rainer Krankenhagen [2], Davide Palumbo [1], Philipp D. Hirsch [2] and Umberto Galietti [1,*]

[1] Department of Mechanics, Mathematics and Management (DMMM), Polytecnic University of Bari, Via Orabona 4, 70125 Bari, Italy; ester.daccardi@poliba.it, davide.palumbo@poliba.it, umberto.galietti@poliba.it
[2] Bundesanstalt für Materialforschung und -prüfung (BAM), Unter den Eichen 87, 12205 Berlin, Germany; rainer.krankenhagen@bam.de, philipp-daniel.hirsch@bam.de, julien.lecompagnon@bam.de
* Correspondence: ester.daccardi@poliba.it
† Presented at the 18th International Workshop on Advanced Infrared Technology and Applications (AITA), Kobe, Japan, 15–19 September 2025.

Abstract: In additive manufacturing (AM), particularly with AlSi10Mg aluminum alloy produced via Laser Powder Bed Fusion (L-PBF), understanding and detecting defects is crucial for ensuring mechanical integrity. This study evaluates the effectiveness of active thermography as a fast, non-destructive testing (NDT) method for identifying typical L-PBF defects. Artificial defects (cubes, spheres, cylinders with unfused powder) were introduced by varying printing parameters. Their real geometry was assessed via micro-computed tomography (μ-CT), revealing deviations from nominal shapes. Thermographic tests using a laser heat source (≈40 W/cm²) were conducted to examine the detectability of these defects in this highly diffusive material AlSi10Mg. Results highlight both the limitations and potential of thermography as a cost- and time- effective alternative to μ-CT for quantitative inspection.

Keywords: Non-destructive testing; Laser Powder Bed Fusion (L-PBF); laser thermography; Micro-computed tomography; structural integrity.

1. Introduction

Additive manufacturing (AM) builds components layer by layer by depositing material and is increasingly used across various industries to produce parts from plastics, metals, and ceramics. Among metal AM techniques, Laser Powder Bed Fusion (L-PBF) is popular for manufacturing high-performance components in aerospace, automotive, and medical fields. This process uses a laser to selectively melt thin layers of metal powder until the part is complete [1].

Process parameters like laser power, scanning speed, and powder flow greatly affect the quality of the final product. Variations in these settings can cause defects such as porosity, surface roughness, and thermal cracking. Porosity can arise from keyhole instability at high power densities, lack of fusion between layers, or laser interruptions [2].

Accurate defect detection during and after manufacturing is essential. Micro-computed tomography (μCT) [3] is a reliable reference method for volumetric defect analysis but is expensive, time-consuming, and not suited for extensive industrial inspection. In contrast, thermographic testing (TT) [4] offers rapid, non-contact inspection and can detect surface and subsurface defects. It is less sensitive to surface roughness and adaptable to various heat sources, making it promising for in-line monitoring.

Additive manufacturing allows to produce simulated defects with various shapes that closely resemble real flaws, allowing for the calibration of NDT techniques and the definition of their detection limits [2].

This study aims to evaluate the capability of thermographic testing (TT) not only to detect defects but also to assess how defect shape influences the thermal signal. The investigation focuses on samples of AlSi10Mg alloy produced by L-PBF, a material partic-

Citation: To be added by editorial staff during production.

Academic Editor: Firstname Lastname

Published: date

ularly challenging for thermal inspections due to its high thermal diffusivity. Using micro-computed tomography (μCT) as a reference method alongside TT, the results highlight the potential of thermography to evolve into a reliable and quantitative inspection tool for additive manufacturing parts [5].

2. Material and methods

The specimens are rectangular parallelepipeds with overall dimensions of 26 × 26 × 2.65 mm³ (Figure 1a and b), containing internal artificial defects of three different shapes, all filled with unmolten powder. Each defect has nominal in-plane dimensions of either 2 × 2 mm² or 1 × 1 mm², and heights respectively of 2 or 1 mm. In the first configuration (NDT-1), the defects are cylindrical; in the second (NDT-2), they are cube-shaped; and in the third (NDT-3), they are spherical, inscribed within the corresponding cubes used in NDT-2. Figure 1c illustrates the size relationships; in particular, the different defect shapes represent defects with similar lateral extent but differing volumes (maximum values): V(cube) = 8 mm³ > V(cylinders) = 6.3 mm³ > V(spheres) = 4.2 mm³. For all defect types, the reported depth refers to the distance from the top surface of the specimen to the uppermost surface of the defect, i.e., the point where the defect begins (Figure 1c). The defect depth ranges from 0.10 mm to 0.55 mm with a step of 0.05 mm.

The samples were manufactured using the L-PBF process with AlSi10Mg aluminum alloy. Standard processing parameters were adopted, including a layer thickness of 30 μm, a laser power of 370 W, a scanning speed of 1280 mm/s, and a hatch distance of 0.13 mm, resulting in a volumetric energy density of 74.12 J/mm². The artificial defects were introduced by intentionally omitting the melting of specific areas during the printing process, thereby simulating internal voids.

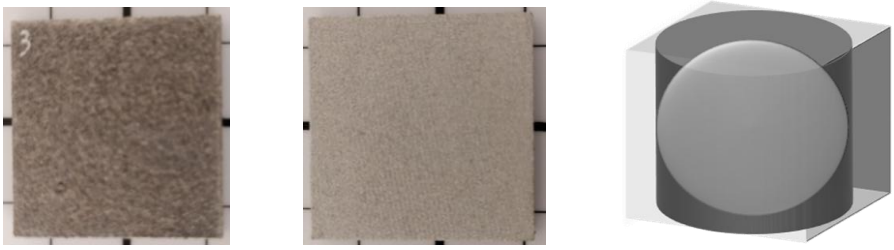

(a) (b) (c)

Figure 1. (a) Front specimen surface, (b) rear specimen surface and (c) a simple schematization of defect geometry.

Thermographic tests were performed in a reflection setup (Figure 2) using a MWIR VELOX 327k SM from IRCAM camera with a cooled sensor (NEDT < 29 mK). A 50 mm lens combined with extension rings provided a spatial resolution of 0.1 mm/pixel. The camera operates in fullframe at 1004 Hz. Due to the high-speed test the window height was limited to 240 px with 2000 Hz. The width was cut to 240 px with respect of the sample size. In this configuration, based on available calibration ranges, an integration time of 470 μs was adopted for the acquisitions.

A 500 W diode laser (900–1080 nm) with a 34 × 34 mm² square optic was used as the heat source, delivering ~40 W/cm². For a coaxial measurement, a 45° dichroic mirror was placed between the camera and the specimen. Step thermography with 1 s long pulses was applied to evaluate the thermal response during heating.

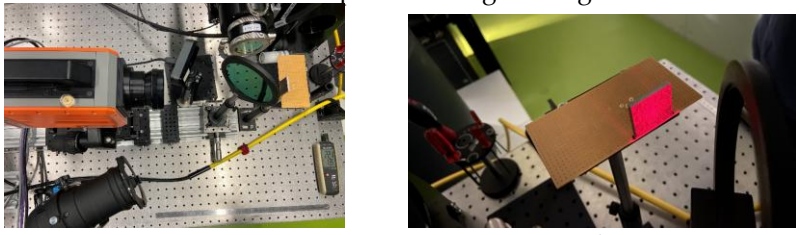

(a) (b)

Figure 2. (a) Reflection experimental set-up used for the stepped laser thermography. (b) Particular view of laser excitation (pilot laser) on specimen front surface.

For reference and comparison with the thermographic tests, tomographic analyses were performed using a Nikon 225MCT system. This high-resolution X-ray micro-computed tomography system is equipped with a 225 kV microfocus source, capable of delivering up to 225 W of power. A voxel size of 15 µm was achieved using a 2000 × 2000 pixels flat panel detector with a pixel pitch of 127 µm.

3. Results and discussion

As demonstrated in previous works from the same authors [6], in L-PBF samples, the characteristic surface roughness leads to non-uniform emissivity, non-uniform absorption of the laser light and hot spots on partially outstanding grains, which generate thermal contrasts unrelated to subsurface defects. These effects influence the transient response and hinder accurate defect detection (Figures 3a and b).

During heating, a change in the dominant heat flow regimes at the sample takes place. Initially, during the very early period (within about 20 ms, the Parker time for the full thickness), deviations from a linear thermal response occur due to transient heat flow. After approximately 100 ms, the specimen becomes thermally thin [2] characterized by a linear temporal response (Figure 3c). The wavy substructure of the curve is probably due to the working frequency of the Stirling cooler.

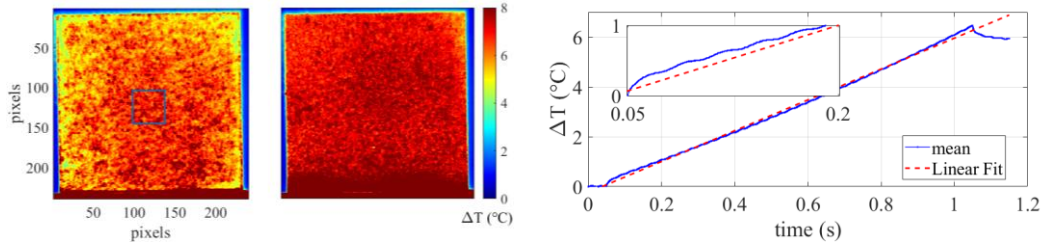

Figure 3. A thermogram from the specimen NDT-2 recorded at the end of the heating period for both (a) front and (b) rear surfaces and (c) related apparent temperature transient of the indicated ROI (blue square) – front side, emissivity 1 (standard test measurements [6] revealed an average emissivity value of approximately 0.3 for this grain surface.).

Proper post-processing of thermographic data is therefore essential. For this purpose, phase evaluation was employed, as it is less sensitive to surface-related artifacts and emissivity variations than traditional thermal contrast methods. Following preliminary analyses based on Fast Fourier Transform (FFT), the dominant frequency component was effectively captured by the first harmonic. A sequence of 256 frames (approximately 120 ms) was analyzed, focusing on the phase results at 7.8 Hz. Figure 4a-c shows an example of the results for the 3 different defect geometries, considering the inspected rear surface (deeper defects). The analysis was conducted at this specific frequency, and the normalized phase contrast results are presented. The normalization was performed using a reference area at the bottom of the image, free of thermal prints or defect signals, by calculating the mean and standard deviation within that region.

Considering all the defect geometries, Figures 4d, e and f show the reference µ-CT results, taking a slice a distance from rear surface of 2 mm. The tomographic images revealed that all defects are indeed present, although they are smaller than expected and their shapes deviate from the originally planned geometry [5].

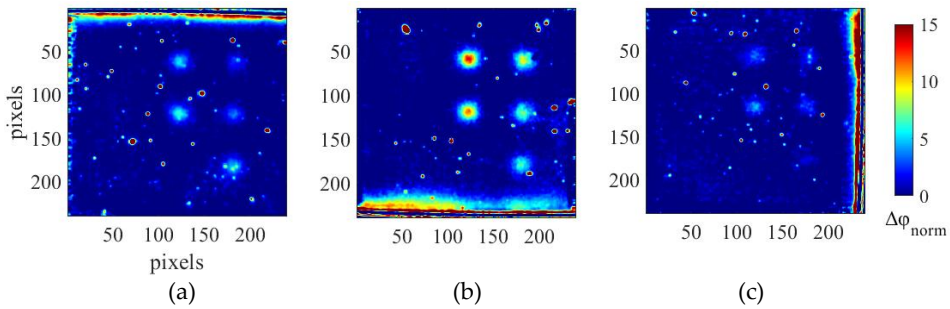

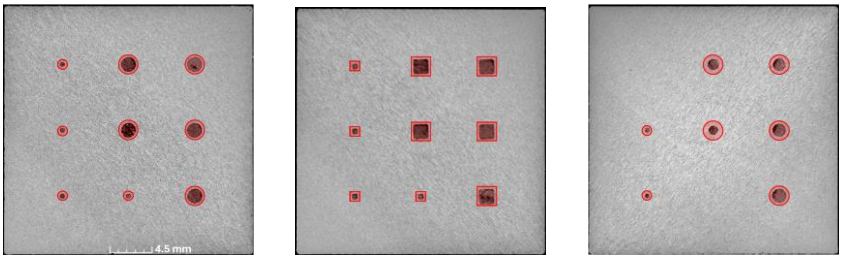

(d) (e) (f)

Figure 4. Phase result at 7.8 Hz after normalization for the 3 different defect geometries and specifically (a) cylinders NDT-1, (b) cubes NDT-2, (c) spheres NDT-3, and reference μ-CT results for the same samples, (d) NDT-1, (e) NDT-2 and (f) NDT-3 considering a slice at a distance from rear surface of 2 mm. N.B. Due to the actual depths and volumes of the spherical defects, it is not possible to represent all of them within the same slice. Nevertheless, all the smaller spheres have been generated.

4. Conclusions and outlook

Within the presented study it could be shown that pulsed laser thermography is able to detect inner manufacturing defects in AlSi10Mg when a fast infrared camera (framerate of about 2 kHz) is used. However, the detection was successful only for defects with volumes of about 5 mm³ (maximum depth 0.55 mm), but not for defect volumes below 1 mm³ (minimum depth 0.10 mm). Future works will consider the specific defect shapes from the μ-CT investigations in correlation to the detected thermal signals. The final goal is an understanding of the observed detection limit for those internal defects, as a result from the interaction between material, geometry, heating process and infrared detection of the apparent surface temperature.

Author Contributions: Conceptualization, E.D., R.K.; methodology, E.D., R.K., D.P., U.G.; formal analysis, E.D.; investigation, E.D., R.K., D.P., U.G.; resources, U.G.; data curation, E.D., P.H.; writing—original draft preparation, E.D.; writing—review and editing, E.D., R.K., D.P., U.G., P.H.; supervision, U.G.; project administration, U.G.; funding acquisition, U.G. All authors have read and agreed to the published version of the manuscript.

Funding: This research was funded by the project TO ZERO - Towards Zero Waste In Aluminium Body-In-White Manufacturing a valere sulle agevolazioni previste dal Decreto Ministeriale 31 dicembre 2021 (Primo sportello) del MIMIT – Accordi per l'innovazione, CUP: B99J23002030005.

Conflicts of Interest: "The authors declare no conflicts of interest."

Acknowledgments: The authors gratefully acknowledge Valland S.r.l. for specimen production and Agiometrix S.r.l. for providing tomographic data during a consultancy activity with PoliBa.

References

1. Limbasiya, N., Jain, A., Soni, H., Wankhede, V., Krolczyk, G., & Sahlot, P. (2022). A comprehensive review on the effect of process parameters and post-process treatments on microstructure and mechanical properties of selective laser melting of AlSi10Mg. *Journal of Materials Research and Technology*, *21*, 1141-1176.
2. Krankenhagen, R., & Maierhofer, C. (2014). Measurement of the radiative energy output of flash lamps by means of thermal thin probes. *Infrared physics & technology*, *67*, 363-370.
3. Ulbricht, A., Mohr, G., Altenburg, S. J., Oster, S., Maierhofer, C., & Bruno, G. (2021). Can potential defects in LPBF be healed from the laser exposure of subsequent layers? A quantitative study. *Metals*, *11*(7), 1012.
4. Maldague, X. (2001). Theory and practice of infrared technology for nondestructive testing.
5. D'Accardi, E., Krankenhagen, R., Ulbricht, A., Pelkner, M., Pohl, R., Palumbo, D., & Galietti, U. (2022). Capability to detect and localize typical defects of laser powder bed fusion (L-PBF) process: An experimental investigation with different non-destructive techniques. *Progress in Additive Manufacturing*, *7*(6), 1239-1256.
6. ASTM E1933-14(2022), *Standard Test Method for Measuring and Compensating for Emissivity Using Infrared Imaging Radiometers*, ASTM International, West Conshohocken, PA, 2022. DOI: https://doi.org/10.1520/E1933-14R22
7. D'Accardi, E., Ulbricht, A., Krankenhagen, R., Palumbo, D., & Galietti, U. (2021, February). Capability of active thermography to detect and localize pores in Metal Additive Manufacturing materials. In *IOP conference series: materials science and engineering* (Vol. 1038, No. 1, p. 012018). IOP Publishing.